Micromechanical modeling of smart composites considering debonding of reinforcements

Yasser M. Shabana [a,*], Matti Ristinmaa [b]

[a] Mechanical Design Department, Faculty of Engineering, El-Mataria, Helwan University, P.O. Box 11718, Cairo, Egypt
[b] Division of Solid Mechanics, Lund University, P.O. Box 118, 221 00 Lund, Sweden

ARTICLE INFO

ABSTRACT

Using the information of the microstructure, this paper presents the development of an incremental constitutive law governing the response of an electro-magneto-thermo-mechanical smart composite. In this development, different shapes of reinforcements that have magneto-electro-thermo-elastic properties that differ from the matrix material are considered. Shapes such as ellipsoidal (spherical, prolate and oblate) particles, elliptical and circular cylindrical fibers, disk and ribbon can be treated provided that the corresponding Eshelby tensor is used. The debonding of the reinforcements from the matrix is also a part of the microscopic process considered. The developed incremental constitutive law not only predicts the macroscopic and microscopic electro-magneto-thermo-mechanical-elastic behavior of composites while considering the debonding process, but it also characterizes their different macroscopic effective properties such as permittivity, permeability, stiffness moduli, pyroelectricity, pyromagnitivity and thermal expansion coefficient in different directions. Moreover, the developed constitutive law is applicable to porous materials and composites with multiple reinforcements and porosities. In the two examples considered below, particular attention is devoted to assessing the effects of both the shape and the concentration of the inclusion and/or porosity and the damage evolution on the multiphysical microscopic and macroscopic behaviors and the effective properties. The first example sheds light on obtaining the macroscopic effective properties, taking into account the piezoelectric $BaTiO_3$ continuous fibers embedded in the piezomagnetic $CoFe_2O_4$ matrix. While in the second example, mechanical loading is considered, epoxy is taken as the matrix material and the response of the composite is presented while the evolution of damage in terms of debonding is taking place.

© 2011 Elsevier Ltd. All rights reserved.

1. Introduction

Composite materials consisting of piezoelectric and piezomagnetic phases have drawn a significant interest due to the rapid development in adaptive material systems. However, the increased complexity of the microstructure in these materials complicates their analysis. One possible route to solve such complexity is to achieve useful models that calculate the effective material properties. Therefore, many studies were concerned with the prediction of the effective or overall properties using various techniques. For instance, Aboudi (2001) employed a homogenization micromechanical method to predict the effective moduli of electro-magneto-thermo-elastic composites. Results for fibrous and periodically bilaminated composites were compared with the generalized method of cells and the Mori–Tanaka predictions. Li and Dunn (1998b) developed a micromechanical approach to analyze the average fields and effective properties of heterogeneous

media that exhibit full coupling between stationary elastic, electric and magnetic fields. Using the solutions obtained for inclusion and inhomogeneity problems in an infinite magneto-electro-elastic medium (Li and Dunn, 1998a), they established exact relations for the internal field distribution inside a heterogeneous magneto-electro-elastic solid. In addition, they obtained closed-form expressions for the effective moduli of fibrous and laminated composites as well as the exact connections between the effective thermal moduli and the effective magneto-electro-elastic moduli of two-phase composites. Li (2000) studied the average magneto-electro-elastic field in a multi-inclusion or an inhomogeneity embedded in an infinite matrix and developed a numerical algorithm to evaluate the magneto-electro-elastic Eshelby tensors for the general material symmetry and ellipsoidal inclusion. Based on the framework of the Variational Asymptotic Method for Unit Cell Homogenization (VAMUCH), Tang and Yu (2009) developed a micromechanics approach to predict the effective properties as well as the local fields of periodic smart materials responsive to fully coupled electric, magnetic, thermal and mechanical fields.

Voids exist in smart materials and some inclusions may be partially or fully debonded from the matrix. These can be attributed to

* Corresponding author. Tel.: +2 (02) 24942176; fax: +2 (02) 26332398.
   E-mail addresses: yasser.shabana@gmail.com (Y.M. Shabana), matti.ristinmaa@solid.lth.se (M. Ristinmaa).

either the manufacturing process or the loading conditions during the usage of a smart material. Therefore, the effects of defects and inclusions on the properties of smart materials are important to be considered. Zhong and Meguid (1997) developed a generalized and mathematically rigorous model to treat the partially debonded circular inhomogeneity problem in piezoelectric materials under anti-plane shear and in-plane electric field using the complex variable method. This enabled the explicit determination of the complex potentials inside the inhomogeneity and the matrix. Deng and Meguid (1999) dealt with the problem of a partially debonded piezoelectric circular inclusion in a piezoelectric matrix and derived the closed form complex potentials both inside and outside the inclusion. They explicitly derived the formulae for the electro-elastic field intensity factors of the interfacial crack. Chung and Ting (1996) studied the two dimensional problems of an elliptic hole or inclusion in a solid of an isotropic piezoelectric material. Fang et al. (2010) presented a theoretical method to study the multiple scattering of electro-elastic waves resulting from two subsurface holes in a functionally graded piezoelectric material layer bonded to a homogeneous piezoelectric material, and also presented the dynamic stress around the holes.

Based on the above introduction, it is evident that predicting the response of a smart material while considering its microstructure is both theoretically challenging and practically important. The need for estimating the electro-magneto-thermo-mechanical elastic behavior of smart composite structures while considering damage evolution and different geometries of the reinforcements has naturally arisen as smart composites are increasingly used in different engineering applications. Accordingly, the aim of this work is to present a micromechanically-based model and its corresponding incremental constitutive law for a smart heterogeneous composite while considering the damage evolution. The damage evolution is presented by the debonding of the inclusions from the matrix. This model incorporates the full coupling of electric, magnetic, thermal and elastic mechanical behaviors. In addition, the resulting incremental constitutive law is able to calculate the local microscopic fields in the matrix and in the inclusion as well as the macroscopic field. Moreover, it can predict the effective properties including the effective elastic, piezoelectric, piezomagnetic, dielectric, magnetic permeability and magneto-electric coupling coefficients as well as the thermal stress coefficients and the associated pyroelectric and pyromagnetic constants. Taking the debonding process into consideration, this constitutive law is applicable to porous materials and composites with multiple reinforcements and porosities including a wide range of inclusion and/or pore geometries ranging from elliptical cylinder to thin disk to sphere to ribbon provided that the proper Eshelby tensor is used. To validate the predictions of the proposed model, the results are compared to those obtained from the following four approaches: the homogenization theory, the generalized method of cells and the Mori–Tanaka approach – all presented by Aboudi (2001) – and the results based on the VAMUCH of Tang and Yu (2009). Agreements between these five approaches have been shown to be very good.

2. Properties of the constituent materials

Electro-magneto-thermo-elastic media that exhibit linear, static, anisotropic coupling between the magnetic, electric, thermal and elastic fields are considered. In this case, the constitutive equations for both the matrix and reinforcements can be expressed as follow:

$$\sigma_{ij} = C_{ijkl}\varepsilon_{kl} + e_{ijl}(-E_l) + q_{ijl}(-H_l) - \lambda_{ij}\,dT$$
$$D_i = e_{ikl}\varepsilon_{kl} - k_{il}(-E_l) - a_{il}(-H_l) - p_i\,dT \qquad (1)$$
$$B_i = q_{ikl}\varepsilon_{kl} - a_{il}(-E_l) - \mu_{il}(-H_l) - m_i\,dT$$

Here σ_{ij} and ε_{ij} are the stress tensor and strain tensor, respectively; D_i and E_i are the electric displacement and electric field; B_i and H_i are the magnetic flux and field. C_{ijkl}, k_{il}, and μ_{il} are the elastic stiffness, the dielectric, and magnetic permeability tensors, respectively. Stress is coupled with the electric and magnetic fields through the piezoelectric, e_{ijl}, and piezomagnetic, q_{ijl}, coefficients, respectively, while electric and magnetic fields are coupled through the magneto-electric coefficient, a_{il}. Finally, the stress, electric displacement, and magnetic flux are coupled with temperature changes dT through the thermal stress tensor λ_{ij} (note that $\lambda_{ij} = C_{ijkl}\alpha_{kl}$ with α_{kl} as the thermal expansion strain tensor), pyroelectric coefficient p_i, and pyromagnetic coefficient m_i.

In order for the different multiphysical properties of the smart materials to be readily computed, the theoretical estimates are developed using a matrix formulation. Hence, the constitutive equation (1) is written in matrix form as follows:

$$\begin{bmatrix} \sigma \\ D \\ B \end{bmatrix} = \begin{bmatrix} C & e & q \\ e^T & -k & -a \\ q^T & -a^T & -\mu \end{bmatrix} \begin{bmatrix} \varepsilon \\ -E \\ -H \end{bmatrix} - \begin{bmatrix} \lambda \\ p \\ m \end{bmatrix} dT \qquad (2)$$

where using the symmetry of the stress and strain tensors, $\boldsymbol{C}$ is a 6×6 submatrix for elastic constants, $\boldsymbol{e}$ is a 6×3 submatrix for piezoelectric coefficients, $\boldsymbol{q}$ is a 6×3 submatrix for piezomagnetic coefficients. Moreover, $\boldsymbol{k}$ is a 3×3 submatrix for dielectric coefficients, $\boldsymbol{a}$ is a 3×3 submatrix for electromagnetic coefficients and $\boldsymbol{\mu}$ is a 3×3 submatrix for magnetic permeability.

In the following analysis, it is convenient to treat the elastic, electric, and magnetic fields equally. To this end, the notation introduced by Barnett and Lothe (1975) for piezoelectric analysis and then generalized to incorporate magnetic coupling by Alshits et al. (1992) is utilized. Here, only the matrix formats are considered, but more details can be found in Li and Dunn (1998b). The generalized stress Σ is introduced as a 12×1 column matrix containing the global stress, global electric displacement and global magnetic flux as

$$\boldsymbol{\Sigma} = [\,\sigma_{11} \quad \sigma_{22} \quad \sigma_{33} \quad \sigma_{23} \quad \sigma_{31} \quad \sigma_{12} \quad D_1 \quad D_2 \quad D_3 \quad B_1 \quad B_2 \quad B_3\,]^T$$
$$(3)$$

the superscript T denotes the transpose. The generalized strain $\boldsymbol{Z}$ is defined as a 12×1 column matrix containing the global strains and the electric and magnetic fields as

$$\boldsymbol{Z} = [\varepsilon_{11} \quad \varepsilon_{22} \quad \varepsilon_{33} \quad \gamma_{23} \quad \gamma_{31} \quad \gamma_{12} \quad -E_1 \quad -E_2 \quad -E_3 \quad -H_1 \quad -H_2 \quad -H_3]^T \quad (4)$$

Taking advantage of the generalized formats defined above, allows the constitutive Eq. (2) to be written as

$$\boldsymbol{\Sigma} = \boldsymbol{LZ} - \boldsymbol{\Psi}\,dT = \boldsymbol{L}(\boldsymbol{Z} - \boldsymbol{\Pi}dT) \qquad (5)$$

where $\boldsymbol{L}$ is a 12×12 effective material matrix containing the effective multiphysics material properties and $\boldsymbol{\Psi}$ is a 12×1 matrix containing the second-order thermal stress tensor λ, the vector of pyroelectric $\boldsymbol{p}$ and the vector of pyromagnetic $\boldsymbol{m}$. In addition, $\boldsymbol{\Pi}$ equals $\boldsymbol{L}^{-1}\,\boldsymbol{\Psi}$ and the superscript -1 is used to denote inversion.

For a transversely isotropic piezoelectric-piezomagnetic composite with axis of symmetry oriented in the 3-direction, the material matrix $\boldsymbol{L}$ takes the following form where the coefficients are labeled according to Aboudi (2001) to facilitate an easy comparison with results of other studies in the literature.

$$
L = \begin{bmatrix}
C_{11} & C_{12} & C_{13} & 0 & 0 & 0 & 0 & 0 & e_{31} & 0 & 0 & q_{31} \\
 & C_{11} & C_{13} & 0 & 0 & 0 & 0 & 0 & e_{31} & 0 & 0 & q_{31} \\
 & & C_{33} & 0 & 0 & 0 & 0 & 0 & e_{33} & 0 & 0 & q_{33} \\
 & & & C_{44} & 0 & 0 & 0 & e_{15} & 0 & 0 & q_{15} & 0 \\
 & & & & C_{44} & 0 & e_{15} & 0 & 0 & q_{15} & 0 & 0 \\
 & & & & & C_{66} & 0 & 0 & 0 & 0 & 0 & 0 \\
 & & & & & & -k_{11} & 0 & 0 & -a_{11} & 0 & 0 \\
 & & & & & & & -k_{11} & 0 & 0 & -a_{11} & 0 \\
 & & & & & & & & -k_{33} & 0 & 0 & -a_{33} \\
 & & & & & & & & & -\mu_{11} & 0 & 0 \\
 & & & & & & & & & & -\mu_{11} & 0 \\
 & & & & & & & & & & & -\mu_{33}
\end{bmatrix}
$$

and $\boldsymbol{\Psi}$ is given as

$$
\boldsymbol{\Psi} = \begin{bmatrix} \lambda_{11} & \lambda_{22} & \lambda_{33} & \lambda_{23} & \lambda_{31} & \lambda_{12} & p_1 & p_2 & p_3 & m_1 & m_2 & m_3 \end{bmatrix}^T
$$

From here on, $\boldsymbol{\Sigma}$ and $\boldsymbol{Z}$ will be referred to as excitation field and response field, respectively.

3. Incremental constitutive equation

The incremental formulation is introduced so that the resulting constitutive equation is valid for composites with different properties of the constituents while considering the debonding process of the reinforcements.

3.1. Formulation

In Fig. 1, the piezoelectromagnetic composite of interest is shown. The states before and after an incremental deformation of the composite containing piezoelectromagnetic elements, in the damage process are depicted. The far field applied mechanical, electrical and magnetic loading conditions are denoted as Σ and the response field as Z^0 at the start of an increment where at the end of the increment the values are given by $\Sigma + d\Sigma$ and $Z^0 + dZ^0$. Moreover, the state before the incremental deformation, shown in Fig. 1(a), is described in terms of the volume fractions of the in-

Intact particle volume fraction: f_p
Debonded particle volume fraction: f_d
Matrix volume fraction: $1 - f_p - f_d$

Intact particle: $f_p - df_p$
Debonded particle: $f_d + df_p$
Matrix: $1 - f_p - f_d$

(a) Before incremental deformation

(b) After incremental deformation

Fig. 1. Debonding of inhomogeneities in the deformation process.

tact and damaged particles f_p and f_d. If the volume fraction of the particles that are debonded during the incremental deformation is denoted by df_p, then the state after deformation, shown in Fig. 1(b), can be described in terms of the volume fractions of the intact and debonded particles $f_p - df_p$ and $f_d + df_p$.

To obtain the incremental macroscopic and microscopic constitutive responses, the analyses will be based on the formulation provided by Tohgo and Chou (1996) and Shabana (2003) for the debonding case. Following Eshelby equivalence principle combined with Mori–Tanaka mean field concept, the incremental excitation field in the intact particle, $d\Sigma^p$, is given by

$$
\begin{aligned}
d\boldsymbol{\Sigma^p} &= d\boldsymbol{\Sigma} + d\widetilde{\boldsymbol{\Sigma}} + d\boldsymbol{\Sigma}_1^{pt} = \boldsymbol{L}_1\left(d\boldsymbol{Z}^0 - \Pi_1 dT + d\widetilde{\boldsymbol{Z}} + d\boldsymbol{Z}_1^{pt}\right) \\
&= \boldsymbol{L}_0\left(d\boldsymbol{Z}^0 - \Pi_0 dT + d\widetilde{\boldsymbol{Z}} + d\boldsymbol{Z}_1^{pt} - d\boldsymbol{Z}_1^*\right)
\end{aligned} \quad (6)
$$

where the subscript 0 refers to the matrix and 1 refers to the reinforcements.

Since air has a significantly smaller dielectric constant relative to that of a piezoelectric material (Sosa, 1992), it is assumed that the excitation field (i.e. the stress, electric displacement and magnetic flux) inside a void vanishes. Hence, the Eshelby equivalence principle for the debonded reinforcement can be written in the following form:

$$
0 = d\boldsymbol{\Sigma} + d\widetilde{\boldsymbol{\Sigma}} + d\boldsymbol{\Sigma}_2^{pt} = \boldsymbol{L}_0\left(d\boldsymbol{Z}^0 - \Pi_0 dT + d\widetilde{\boldsymbol{Z}} + d\boldsymbol{Z}_2^{pt} - d\boldsymbol{Z}_2^*\right) \quad (7)
$$

Furthermore, since in the debonding process the current reinforcement excitation field should be released in the next incremental deformation, the following equation is obtained:

$$
\begin{aligned}
-\boldsymbol{\Sigma^p} &= d\boldsymbol{\Sigma} + d\widetilde{\boldsymbol{\Sigma}} + \boldsymbol{\Sigma}_3^{pt} = \boldsymbol{L}_1\left(d\boldsymbol{Z}^0 - \Pi_1 dT + d\widetilde{\boldsymbol{Z}} + Z_3^{pt}\right) \\
&= \boldsymbol{L}_0\left(d\boldsymbol{Z}^0 - \Pi_0 dT + d\widetilde{\boldsymbol{Z}} + \boldsymbol{Z}_3^{pt} - \boldsymbol{Z}_3^*\right)
\end{aligned} \quad (8)
$$

In the above equations, $d\boldsymbol{\Sigma}$ and $d\widetilde{\boldsymbol{\Sigma}}$ are the incremental excitation field and the incremental average excitation field based on Mori and Tanaka mean field concept, and they are related to $d\boldsymbol{Z}^0$ and $d\widetilde{\boldsymbol{Z}}$ by

$$
d\boldsymbol{\Sigma} = \boldsymbol{L}_0(d\boldsymbol{Z}^0 - \Pi_0 dT), \quad d\widetilde{\boldsymbol{\Sigma}} = \boldsymbol{L}_0 d\widetilde{\boldsymbol{Z}} \quad (9)
$$

In Eqs. (6)–(8), $d\boldsymbol{\Sigma}_1^{pt}$, $d\boldsymbol{\Sigma}_2^{pt}$, $\boldsymbol{\Sigma}_3^{pt}$ and $d\boldsymbol{Z}_1^{pt}$, $d\boldsymbol{Z}_2^{pt}$, $\boldsymbol{Z}_3^{pt}$ represent the perturbed parts of the excitation and the response fields in the intact and debonded reinforcements and the reinforcement to be debonded, respectively. Moreover, $d\boldsymbol{Z}_1^*$, $d\boldsymbol{Z}_2^*$ and $\boldsymbol{Z}_3^*$ are the Eshelby equivalent transformation response fields. The perturbed response fields are related to the transformation response fields by

$$
d\boldsymbol{Z}_1^{pt} = \boldsymbol{S} d\boldsymbol{Z}_1^*, \quad d\boldsymbol{Z}_2^{pt} = \boldsymbol{S} d\boldsymbol{Z}_2^*, \quad \boldsymbol{Z}_3^{pt} = \boldsymbol{S}\boldsymbol{Z}_3^* \quad (10)
$$

where $d\boldsymbol{\Sigma}_1^{pt}$, $d\boldsymbol{\Sigma}_2^{pt}$ and $\boldsymbol{\Sigma}_3^{pt}$ are described by

$$
d\boldsymbol{\Sigma}_1^{pt} = \boldsymbol{L}_0(\boldsymbol{S} - \boldsymbol{I})d\boldsymbol{Z}_1^*, \quad d\boldsymbol{\Sigma}_2^{pt} = \boldsymbol{L}_0(\boldsymbol{S} - \boldsymbol{I})d\boldsymbol{Z}_2^*, \quad \boldsymbol{\Sigma}_3^{pt} = \boldsymbol{L}_0(\boldsymbol{S} - \boldsymbol{I})\boldsymbol{Z}_3^* \quad (11)
$$

The matrix $\boldsymbol{I}$ is a 12×12 identity matrix and the matrix S denotes the magneto-electro-elastic Eshelby tensor of the particles, which is the key ingredient necessary for determining the magnetoelectric coupling of piezoelectric-piezomagnetic composites (Wu and Huang, 2000). For ellipsoidal inclusions, $\boldsymbol{S}$ is expressed as a function of the shape of the inhomogeneity and the electro-magneto-elastic moduli of the matrix. Explicit expressions for the electro-magneto-elastic Eshelby tensors are given in Li and Dunn (1998a) and Huang et al. (1998).

Since the incremental overall excitation field $d\boldsymbol{\Sigma}$ is determined by the average excitation field of the composite, it follows that,

$$
d\boldsymbol{\Sigma} = (f_p - df_p)d\boldsymbol{\Sigma^p} - df_p\boldsymbol{\Sigma^p} + (1 - f_p - f_d)(d\boldsymbol{\Sigma} + d\widetilde{\boldsymbol{\Sigma}}) \quad (12)
$$
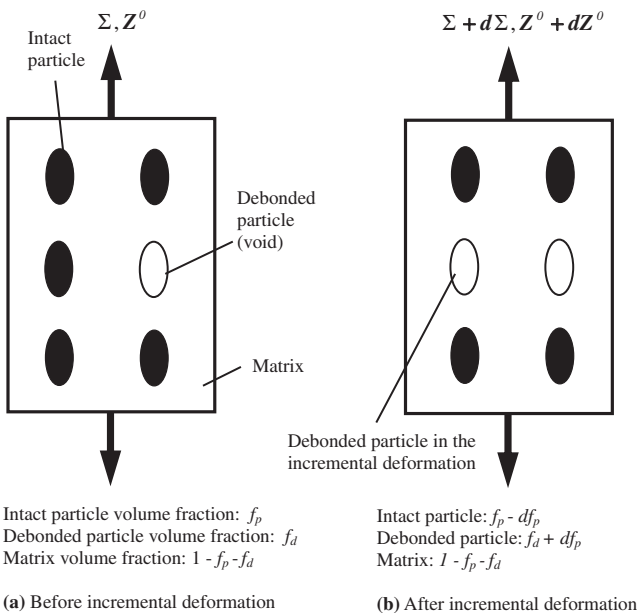
where the incremental average excitation field $d\widetilde{\Sigma}$ is given by

$$d\widetilde{\Sigma} = -\left\{(f_p - df_p)d\Sigma_1^{pt} + f_d d\Sigma_2^{pt} + df_p\Sigma_3^{pt}\right\} \tag{13}$$

Substituting Eqs. (9) and (11) into (13), the incremental average response field is expressed by

$$d\widetilde{Z} = -(S - I)\left\{(f_p - df_p)dZ_1^* + f_d dZ_2^* + df_p Z_3^*\right\} \tag{14}$$

Using Eqs. (6)–(8) and taking Eqs. (10) and (14) into consideration, the following relations are obtained after some mathematical manipulations.

$$L_0^{-1}\Sigma^p = \left[(L_0 - L_1)^{-1}(L_1\Pi_1 - L_0\Pi_0) + \Pi_0\right]dT \\ + \left[S - (L_0 - L_1)^{-1}L_0\right]dZ_1^* - (S - I)Z_3^* \tag{15}$$

$$L_0^{-1}\Sigma^p = (S - I)dZ_2^* - (S - I)Z_3^* \tag{16}$$

$$-L_0^{-1}\Sigma^p = dZ^0 - \Pi_0 dT - (S - I)\left\{(f_p - df_p)dZ_1^* + f_d dZ_2^* + df_p Z_3^*\right\} \\ + (S - I)Z_3^* \tag{17}$$

The Eshelby equivalent transformation response fields, dZ_1^*, dZ_2^* and Z_3^*, are obtained by solving the simultaneous Eqs. (15)–(17). In the general case, there are three phases for the reinforcements in the composite, and there are twelve components of the transformation response field for each phase. The solution can be written as

$$dZ_1^* = \left\{A_1^{-1}B_1 + A_1^{-1}B_1(S - I)H^{-1}df_p[I - (S - I)D_1]\right\}\left(L_0^{-1}d\Sigma + \Pi_0 dT\right) \\ + A_1^{-1}B_1(S - I)H^{-1}L_0^{-1}df_p\Sigma^p - \left\{A_1^{-1}M_1 + A_1^{-1}B_1(S - I)H^{-1}df_p \\ \times [\Pi_0 - (S - I)D_2]\right\}dT$$

$$dZ_2^* = \left\{A_2^{-1}B_2 + A_2^{-1}B_2(S - I)H^{-1}df_p[I - (S - I)D_1]\right\}\left(L_0^{-1}d\Sigma + \Pi_0 dT\right) \\ - A_2^{-1}B_2(S - I)H^{-1}L_0^{-1}df_p\Sigma^p \\ + \left\{A_2^{-1}M_2 - A_2^{-1}B_2(S - I)H^{-1}df_p[\Pi_0 - (S - I)D_2]\right\}dT \tag{18}$$

$$Z_3^* = H^{-1}[(S - I)D_1 - I]\left(L_0^{-1}d\Sigma + \Pi_0 dT\right) - H^{-1}L_0^{-1}\sigma^p \\ + H^{-1}[\Pi_0 - (S - I)D_2]dT$$

where

$$D_1 = (f_p - df_p)A_1^{-1}B_1 + f_d A_2^{-1}B_2$$

$$D_2 = (f_p - df_p)A_1^{-1}M_1 - f_d A_2^{-1}M_2$$

$$A_1 = (L_1 - L_0)^{-1}R_1 - f_d R_3^{-1}R_2$$

$$B_1 = -f_d R_3^{-1}L_0 - I$$

$$M_1 = -f_d R_3^{-1}L_0\Pi_0 - (L_1 - L_0)^{-1}(L_1\Pi_1 - L_0\Pi_0)$$

$$A_2 = \left\{R_1^{-1}(L_1 - L_0)f_d - R_2^{-1}R_3\right\}(I - S) \tag{19}$$

$$B_2 = -R_2^{-1}L_0 - R_1^{-1}(L_1 - L_0)$$

$$M_2 = R_1^{-1}(L_1\Pi_1 - L_0\Pi_0) + R_2^{-1}L_0\Pi_0$$

$$H = (S - I)(f_p - df_p)A_1^{-1}B_1(S - I)df_p \\ + (S - I)f_d A_2^{-1}B_2(S - I)df_p + (S - I)(1 - df_p)$$

$$R_1 = L_0 + (L_1 - L_0)S + (L_1 - L_0)(I - S)(f_p - df_p)$$

$$R_2 = -L_0(I - S)(f_p - df_p)$$

$$R_3 = L_0(1 - f_d)$$

The incremental overall response field, dZ, of the composite is expressed by the average response field as follows:

$$dZ = (f_p - df_p)\left(dZ^0 + d\widetilde{Z} + dZ_1^{pt}\right) + f_d\left(dZ^0 + d\widetilde{Z} + dZ_2^{pt}\right) \\ + df_p\left(dZ^0 + d\widetilde{Z} + Z_3^{pt}\right) + (1 - f_p - f_d)\left(dZ^0 + d\widetilde{Z}\right) \tag{20}$$

Considering Eqs. (10) and (14), the above relation becomes

$$dZ = dZ^0 + (f_p - df_p)dZ_1^* + f_d dZ_2^* + df_p Z_3^* \tag{21}$$

Substituting from Eq. (18), the overall incremental response field-, dZ, incremental excitation field, $d\Sigma$, relation of the composite is obtained as

$$dZ = L^{-1}d\Sigma + Pdf_p + \Pi dT \tag{22}$$

where

$$L^{-1} = \left\{(I + D_1) - [D_1(S - I) - I]H^{-1}df_p[(S - I)D_1 - I]\right\}L_0^{-1}$$

$$P = [D_1(S - I) - I]H^{-1}L_0^{-1}\Sigma^p$$

$$\Pi = -\left\{\begin{array}{l}D_2 + [D_1(S - I) - I]H^{-1}df_p[\Pi_0 - (S - I)D_2] \\ -\Pi_0((I + D_1) - [D_1(S - I) - I]H^{-1}[(S - I)D_1 - I]df_p)\end{array}\right\} \tag{23}$$

Eq. (22) shows that the incremental macroscopic response field of the composite consists of three main parts: the response field increment due to the excitation field increment, the debonding damage and the temperature change. The effective electro-magneto-mechanical properties of the composite such as elastic, piezoelectric, piezomagnetic, dielectric, magnetic permeability and magneto-electric coupling coefficients can be extracted from the first part. On the other hand, the thermal stress tensor λ and the associated pyroelectric vector, p, and pyromagnetic vector, m, that are included in the thermal matrix Π of the composite can be extracted from the third part. First, it is concluded that

$$\Psi = L\Pi \tag{24}$$

and finally the thermal expansion coefficients in different directions can be evaluated from

$$\alpha = C^{-1}\lambda \tag{25}$$

The approach also allows for the assessment of the microscopic constitutive behavior, i.e. the resulting local excitation field and thereby also allows for the possibility to design failure-safe electro-magneto-thermo-mechanical smart composites. Therefore, the microscopic excitation and response fields of the matrix and reinforcements are introduced here. The incremental average excitation field of the matrix, $d\Sigma^m = d\Sigma + d\widetilde{\Sigma}$, is given by

$$d\Sigma^m = L_0\left[dZ^0 - \Pi_0 dT - (S - I)\left\{(f_p - df_p)dZ_1^* + f_d dZ_2^* + df_p Z_3^*\right\}\right] \tag{26}$$

Using Eq. (18), the explicit expression of the matrix excitation field can be expressed as

$$d\Sigma^m = L_0(I - S)\left\{\left(\begin{array}{l}(I + D_1) - [D_1(S - I) - I]H^{-1} \\ \times [(S - I)D_1 - I]df_p + (I - S)^{-1}S\end{array}\right)L_0^{-1}d\Sigma \\ + [D_1(S - I) - I]H^{-1}df_p L_0^{-1}\Sigma^p \\ - \left(\begin{array}{l}D_2 + [D_1(S - I) - I]H^{-1}df_p[\Pi_0 - (S - I)D_2] \\ + \Pi_0((I + D_1) - [D_1(S - I) - I]H^{-1}[(S - I)D_1 - I]df_p - I)\end{array}\right)\right\}dT \tag{27}$$

Moreover, the incremental average excitation field of the intact reinforcements is

$$d\Sigma^p = d\Sigma + d\widetilde{\Sigma} + d\Sigma_1^{pt} \\ d\Sigma^p = d\Sigma^m + L_0(S - I)dZ_1^* \tag{28}$$

Furthermore, the incremental average response fields of the matrix and both the intact and damaged reinforcements can be evaluated from

$$dZ^m = L_0^{-1} d\Sigma^m$$
$$dZ^p = L_1^{-1} d\Sigma^p \qquad (29)$$
$$dZ^d = dZ^0 + d\widetilde{Z} + SdZ_2^*$$

With Eqs. (27)–(29) and taking advantage of Eq. (18), it is then possible to calculate the incremental microscopic excitation and response fields for the different constituents.

3.2. Volume fraction of the particles in the debonding process

Based on the critical energy criterion of interfacial debonding (Chen et al., 2003), the threshold bond strength σ_{cr} between the particle and matrix materials depends on the particle size and may be written as

$$\sigma_{cr} = \sqrt{\frac{\gamma(1 - f_{po})E_0}{c_1[f_{po}(1 - 2v_0) + (1 + v_0)/2]}} \qquad (30)$$

where γ is the specific interface adhesive energy; E_0 is the initial modulus of the matrix; v_0 is the Poisson ratio of the matrix; c_1 is the particle radius and f_{po} is the initial particle volume fraction.

Suppose the probability of debonding at the interface can be described by the Weibull's distribution function:

$$P = 1 - \exp\left[-\left(\frac{\sigma - \sigma_{cr}}{S_0}\right)^m\right], (\sigma \geqslant \sigma_{cr}) \qquad (31)$$

where S_0 and m are material parameters and σ is the average normal stress at the interface that defined in Chen et al. (2003). Then, for $\sigma > \sigma_{cr}$, the cumulative volume fraction of the damaged reinforcements is represented by $f_{po}P$, and the volume fraction of the reinforcements to be debonded in the incremental deformation, df_p, is given by

$$df_p = f_{po} \frac{dP}{d\sigma} d\sigma \qquad (32)$$

To close the theory, the above relations are then used in the previously-derived constitutive equations of the composite.

4. Numerical results and discussions

In this section, two examples are considered. The intention of the first example is to demonstrate the applicability of the proposed model by applying it to a two-phase electro-magneto-elastic composite consisting of the piezoelectric BaTiO$_3$ continuous fibers embedded in piezomagnetic CoFe$_2$O$_4$ matrix. While in the second example, the matrix is changed to be epoxy instead of CoFe$_2$O$_4$ to evaluate the microscopic and macroscopic fields and the damage evolution of the smart composite under mechanical loading conditions. The electro-magneto-thermo elastic moduli of the constituent materials are taken from Tang and Yu (2009) and are presented in Table 1. The considered materials of the constituents, BaTiO$_3$ and CoFe$_2$O$_4$, are transversely isotropic with the axis of symmetry oriented in the 3-direction while epoxy is isotropic.

4.1. Electro-magneto-thermo elastic properties

Fig. 2 shows the variations of the elastic moduli C_{11} and C_{12} against the volume fraction of the BaTiO$_3$ elliptical cylindrical fibers for different values of the aspect ratio β. It can be seen that both moduli recover the moduli of the constituent phases at the two volume fraction limits. Also, the obtained results are consistent with those presented in Aboudi (2001) for the circular

Table 1
Material properties of the composite constituents (BaTiO$_3$, CoFe$_2$O$_4$ and Epoxy) (Tang and Yu, 2009).

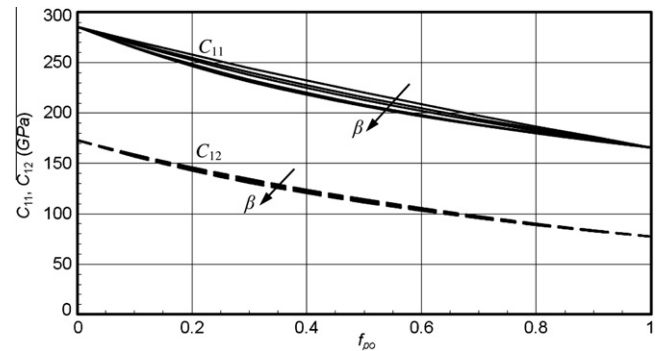|	BaTiO$_3$	CoFe$_2$O$_4$	Epoxy
C_{11} (GPa)	166	286	5.53
C_{12} (GPa)	77	173	2.97
C_{13} (GPa)	78	170	2.97
C_{33} (GPa)	162	269.5	5.53
C_{44} (GPa)	43	45.3	1.28
e_{15} (C m^{-2})	11.6	0	0
e_{31} (C m^{-2})	−4.4	0	0
e_{33} (C m^{-2})	18.6	0	0
k_{11} (10^{-9}C V^{-1} m^{-1})	11.2	0.08	0.1
k_{33} (10^{-9}C V^{-1} m^{-1})	12.6	0.093	0.1
q_{15} (N A^{-1} m^{-1})	0	550	0
q_{31} (N A^{-1} m^{-1})	0	580.3	0
q_{33} (N A^{-1} m^{-1})	0	699.7	0
μ_{11} (10^{-6} N s^2 C^{-2})	5	−590	0.01
μ_{33} (10^{-6} N s^2 C^{-2})	10	157	0.01
α_{11} (×10^{-6} K^{-1})	15.7	10	54
α_{22} (×10^{-6} K^{-1})	15.7	10	54
α_{33} (×10^{-6} K^{-1})	6.4	10	54

Fig. 2. Effective elastic moduli C_{11} and C_{12} of a fibrous composite against the volume fraction of BaTiO$_3$ for different values of the aspect ratio (β = 0.1, 0.5, 1, 5, and 100).

cylindrical fibers (β = 1). While C_{12} is hardly affected by the aspect ratio, C_{11} decreases with its increase. This is mainly because the dimension in the 1-direction of the elliptic cross section of the fiber decreases relative its dimension in the 2-direction with the increase of the aspect ratio and consequently the stiffness decreases in the 1-direction and increases in the 2-direction. Beyond β = 5, the effect of the aspect ratio on C_{11} is negligible. The slight deviation of C_{12} with the aspect ratio may refer to the secondary effect of the electromagnetic properties of the constituents.

Figs. 3–5 reveal the Coefficients of Thermal Expansion (CTEs), pyroelectric p and pyromagnetic m properties as functions of the
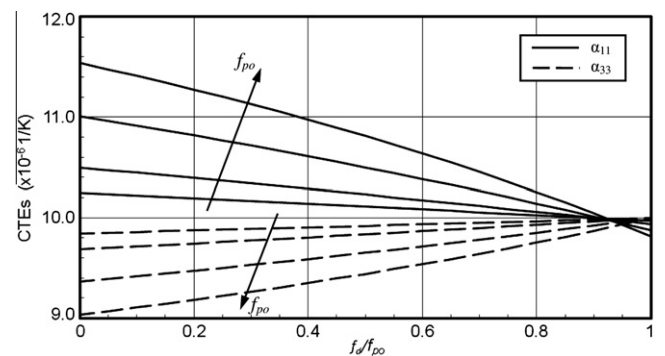
Fig. 3. Effective thermal expansion coefficients α_{11} and α_{33} of a fibrous composite against the damage evolution for different volume fractions of BaTiO$_3$ (f_{po} = 0.05, 0.1, 0.2 and 0.3).
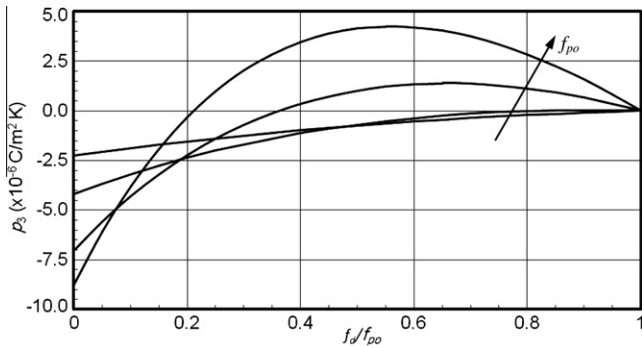
Fig. 4. Effective pyroelectric coefficient p_3 of a fibrous composite against the damage evolution for different volume fractions of BaTiO$_3$ (f_{po} = 0.05, 0.1, 0.2 and 0.3).
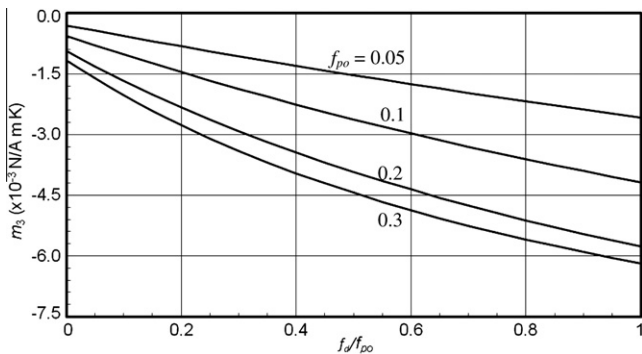

Fig. 5. Effective pyromagnetic coefficient m_3 of a fibrous composite against the damage evolution for different volume fractions of BaTiO$_3$ (f_{po} = 0.05, 0.1, 0.2 and 0.3).

damage evolution f_d/f_{po} due to debonding damage for different values of the circular cylindrical fiber volume fraction. The values of CTEs, p and m coincide with Tang and Yu (2009) when f_d = 0. Since α_{11} of the fiber is higher than both α_{33} and that of the matrix, the increase of the fiber volume fraction results in an increase in α_{11} of the composite and a decrease in its α_{33} as shown in Fig. 3. This behavior occurs because the long fibers prevent the matrix from expanding in the 3-direction, and as a result the matrix is forced to expand more than usual in the transverse directions. This results in a lower CTE in the 3-direction than that in the transverse directions. It can be seen that α_{33} increases when the fibers gradually turn into voids due to the reduction of the fiber volume fraction. This consequently results in more freedom that the matrix has to expand in the 3-direction. When all fibers turn into voids, α_{33} approaches the matrix limit. On the other hand, α_{11} has an opposite behavior as it decreases when fibers gradually turn into voids. Although the pyroelectric and pyromagnetic coefficients are absent in each of the individual constituents, the pyroelectric effect is induced in the composite due to the interaction between the piezoelectric effect and the thermal expansion. Moreover, the pyromagnetic effect is induced due to the interaction between the piezomagnetic effect and the thermal expansion. As depicted in Figs. 4 and 5, the coefficients p_3 and m_3 are in general decreasing with the increase of the fiber volume fraction for the perfect composite (no debonding occurs) and these results are consistent with Tang and Yu (2009). When all fibers turn into voids, p_3 approaches zero for the different values of the fiber volume fraction. On the other hand, m_3 decreases nonlinearly with the damage evolution as shown in Fig. 5.

The electromagnetic coefficient is another material property that is triggered in the composite and can be utilized in practical

applications, even if it is absent in each constituent. The variation of the effective electromagnetic coupling coefficient a_{33} of the fibrous composite against the damage evolution for different volume fractions of the fibers is illustrated in Fig. 6. It can be noticed that a_{33} decreases with the damage evolution and its decreasing rate becomes higher for the higher fiber volume fraction. However, for the perfect composite a_{33} is increasing with the fiber volume fraction and its values are consistent with the results in Aboudi (2001).

Fig. 7 depicts the effective magnetic permeability coefficients μ_{11} and μ_{33} of the smart material against the damage evolution for different volume fractions of the fibers. It can be seen that μ_{11} increases with the increase of the initial fiber volume fraction, which is opposite to μ_{33}. Both coefficients are almost independent on the damage evolution. It can be observed from Fig. 8 that the effective axial dielectric permittivity k_{33} increases significantly with the initial fiber volume fraction, while the effective transverse dielectric permittivity k_{11} is almost independent on the initial fiber volume fraction. Although k_{11} remains almost invariant with the change of the damage evolution, k_{33} decreases almost linearly with the damage evolution.

The variations of the effective piezoelectric coefficients e_{33}, e_{31} and e_{15} are shown in Fig. 9. It is obvious that e_{33} and e_{31} are significant while e_{15} is almost negligible. However e_{33} and e_{31} have opposite behaviors with the increase of the initial fiber volume fraction and the damage evolution; they approach zero when all fibers turn into voids. However the piezomagnetic coefficient q_{15} decreases with the increase of the initial fiber volume fraction as shown in Fig. 10; it is almost independent on the damage evolution. It is found from the numerical results that the other
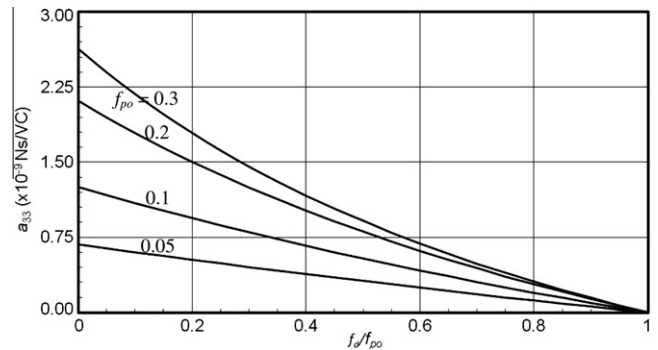

Fig. 6. Effective magnetoelectric coefficient a_{33} of a fibrous composite against the damage evolution for different volume fractions of BaTiO$_3$ (f_{po} = 0.05, 0.1, 0.2 and 0.3).
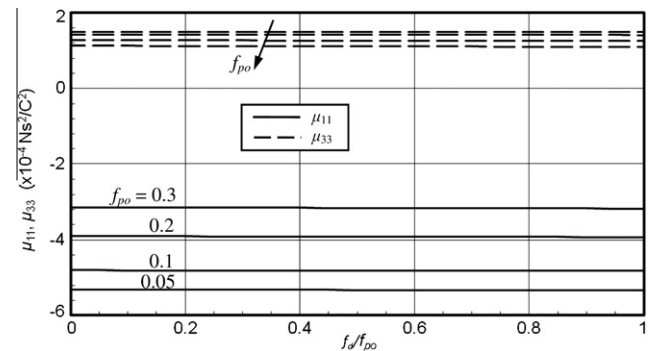

Fig. 7. Effective magnetic permeability coefficient μ_{11} and μ_{33} of a fibrous composite against the damage evolution for different volume fractions of BaTiO$_3$ (f_{po} = 0.05, 0.1, 0.2 and 0.3).
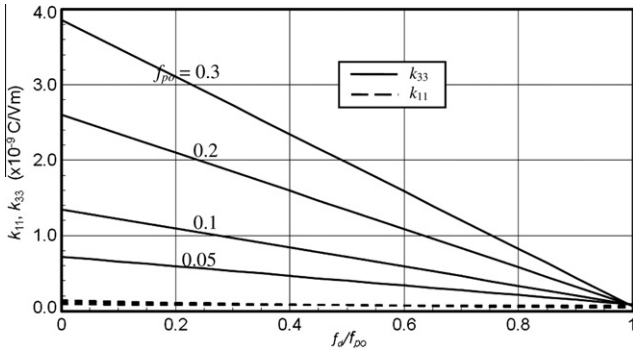
Fig. 8. Effective dielectric coefficients k_{33} and k_{11} of a fibrous composite against the damage evolution for different volume fractions of BaTiO$_3$ (f_{po} = 0.05, 0.1, 0.2 and 0.3).
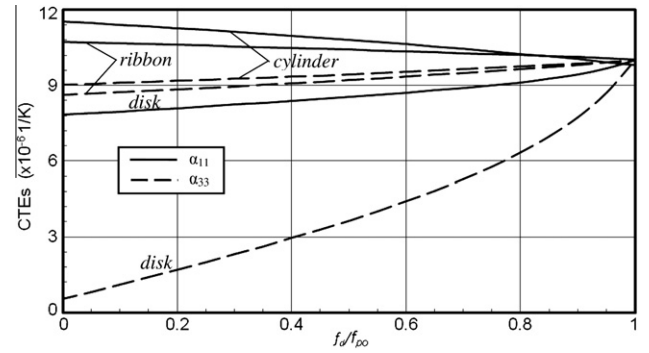

Fig. 11. Effective thermal expansion coefficients α_{11} and α_{33} of a fibrous composite against the damage evolution for different geometries of the reinforcements (f_{po} = 0.3).
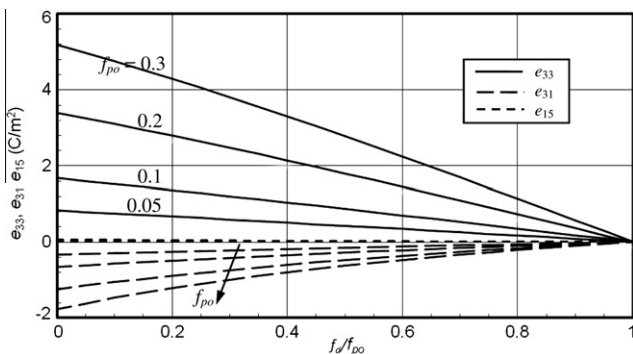

Fig. 9. Effective piezoelectric coefficients e_{33}, e_{31} and e_{15} of a fibrous composite against the damage evolution for different volume fractions of BaTiO$_3$ (f_{po} = 0.05, 0.1, 0.2 and 0.3).
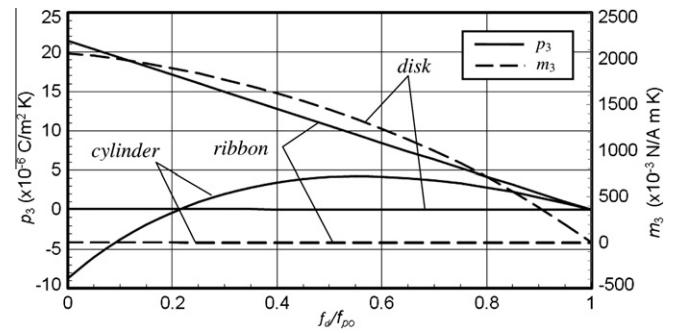

Fig. 12. Effective pyroelectric and pyromagnetic coefficients p_{33} and m_{33} of a fibrous composite against the damage evolution for different geometries of the reinforcements (f_{po} = 0.3).

properties p_3 and m_3 are shown in Fig. 12. The ribbon and thin disk reinforcements have the highest levels for p_3 and m_3 respectively. While disk reinforcement results in negligible p_3, cylinder and ribbon reinforcements result in a negligible m_3 relative to that of the disk reinforcement. Moreover, both properties approach zero when all reinforcements turn into voids. It is emphasized again that the composite exhibits these two properties even if neither constituent exhibits them. It can be seen from the previous results that the different properties have remarkable differences according to the considered reinforcement aspect ratio, volume fraction and geometry.

4.2. Effect of damage evolution during continuous loading

As an example of the application of the present constitutive equation, a continuous loading situation is considered. The purpose of this is to highlight the usefulness of the formulation (e.g. as a constitutive driver in a non-linear finite element setting). The model is evidently very general, but for simplicity the response under uniaxial tension in the axial direction is analyzed. The specific microstructure is described as a particle reinforced smart composite taking into account the debonding damage of the reinforcements. The matrix material is taken as epoxy with the piezoelectric BaTiO$_3$ inclusions. The initial reinforcement volume fraction, the reinforcement diameter and the specific interface adhesive energy are taken to be 0.15, 100 μm and 0.1 J/m^2, respectively.

The variations of the axial stresses in the composite, reinforcement and matrix σ_z, σ_z^p and σ_z^m as well as the damaged reinforcements volume fraction f_d are shown in Fig. 13 as functions of the composite axial strain ε_z. It can be seen that both of the
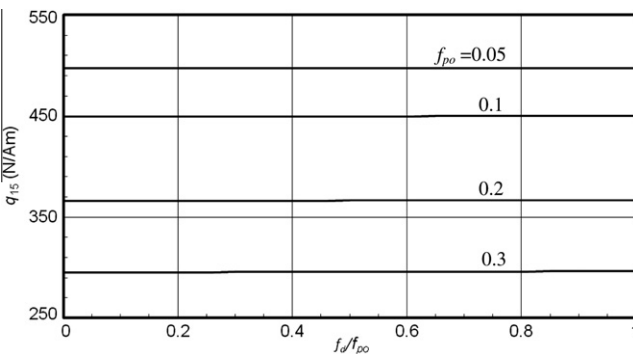

Fig. 10. Effective piezomagnetic coefficients q_{15} of a fibrous composite against the damage evolution for different volume fractions of BaTiO$_3$ (f_{po} = 0.05, 0.1, 0.2 and 0.3).

piezomagnetic coefficients q_{13} and q_{33} have the same order of the magnitude of q_{15} and also have the same behavior of q_{15}.

As a final investigation, three different geometries of the reinforcements are considered in order to investigate their effects on the properties of the smart composite. These geometries are circular cylindrical fiber, thin disk and ribbon with initial volume fraction equals 0.3. It can be seen from Fig. 11 that the transverse CTE α_{11} is higher than the axial one α_{33} for all geometries. In addition, the cylindrical fiber has the highest level for α_{11} and α_{33}, while the disk reinforcement has the lowest one. Moreover, the disk is significantly affected by the damage evolution relative to the other geometries. The variation of the pyroelectric and pyromagnetic
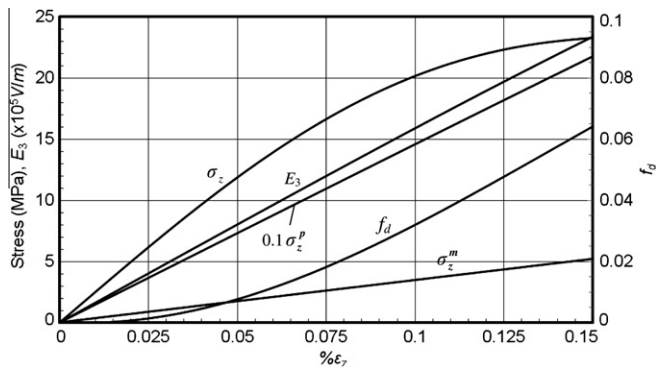
Fig. 13. Microscopic and macroscopic stress–strain relations of the composites with debonding damage. $\beta = 1$, $f_{po} = 0.15$.

microscopic stresses are linear and the reinforcements exhibit the highest linear stress–strain relation while the matrix exhibits the lowest linear one. On the other hand, both the macroscopic stress–strain relation and the damage evolution are nonlinear. Not surprisingly, the volume fraction of the damaged reinforcements increases with the axial strain. It can be noticed that the stress in the reinforcements is one order of magnitude higher than both the stress in the matrix and the macroscopic stress of the composite. Therefore, designing smart structures based on the macroscopic analysis may give misleading results and may lead to unexpected failure of different structures. Eventually, the microscopic analysis and the damage evolution of the reinforcements should be considered when designing different smart structures. For this loading situation, it turns out that the electric field E_3, which is induced due to the piezoelectric effect, increases monotonically with the axial strain as shown in the figure.

5. Conclusions

A micromechanical approach, which results in an incremental constitutive equation, to analyze the local multiphysical microscopic fields in the matrix and in the inclusion as well as the macroscopic multiphysical field of heterogeneous smart composites, which are sensitive to thermomechanical, electric and magnetic fields, is presented. Full coupling between elastic, electric, magnetic and thermal fields and different geometries of the reinforcements as well as the debonding process of the reinforcements due to high loading conditions are considered. The effective multiphysical properties including the effective elastic, piezoelectric, piezomagnetic, dielectric, magnetic permeability and magneto-electric coupling coefficients as well as the thermal stress coefficients and the associated pyroelectric and pyromagnetic constants are extracted from the macroscopic multiphysical field.

The proposed constitutive equation is valid for predicting four different field behaviors of smart composites under four different types of loading conditions either individually or combined. These are electric, magnetic, thermal, and mechanical loading conditions. Also, it is valid for composites that exhibit one or more of these field behaviors and loading conditions. For example, if the composite under consideration is a piezoelectric one with no magnetic

effect of the constituent materials, the proposed constitutive equation can be used after removing the magnetic effect parts; thus, the stiffness and Eshelby matrices will be 9×9 matrices in this case. If the electric parts are also removed, these matrices will be 6×6 matrices and the constitutive equation will deal with the thermo-mechanical behaviors of composites. Moreover, the thermal part can definitely be omitted too leading to predicting the mechanical field behaviors of traditional composites. Eventually, different combinations of the four different fields of different composites can be treated by the proposed constitutive equation.

In short, the presented constitutive law can be used to study the microstructure-property-performance relationship of materials and to guide the design and optimization of the smart structures.

Acknowledgements

References

Aboudi, J., 2001. Micromechanical analysis of fully coupled electro-magneto-thermo-elastic multiphase composites. Smart Mater. Struct. 10, 867–877.

Alshits, V.I., Darinskii, A.N., Lothe, J., 1992. On the existence of surface waves in half-infinite anisotropic elastic media with piezoelectric and piezomagnetic properties. Wave Motion 16, 265–284.

Barnett, D.M., Lothe, J., 1975. Dislocations and line charges in anisotropic piezoelectric insulators. Phys. Status. Solidi B 67, 105–111.

Chen, J.K., Huang, Z.P., Mai, Y.-W., 2003. Constitutive relation of particulate-reinforced viscoelastic composite materials with debonded microvoids. Acta Mater. 51, 3375–3384.

Chung, M.Y., Ting, T.C.T., 1996. Piezoelectric solid with an elliptic inclusion or hole. Int. J. Solids Struct. 33, 3343–3361.

Deng, W., Meguid, S.A., 1999. Closed form solutions for partially debonded circular inclusion in piezoelectric materials. Acta Mech. 137, 167–181.

Fang, X.Q., Liu, J.X., Wang, X.H., Zhang, L.L., 2010. Dynamic stress around two holes buried in a functionally graded piezoelectric material layer under electro-elastic waves. Phil. Mag. Lett. 90, 361–380.

Huang, J.H., Chiu, Y.H., Liu, H.K., 1998. Magneto-electro-elastic Eshelby tensors for a piezoelectric-piezomagnetic composite reinforced by ellipsoidal inclusions. J. Appl. Phys. 83, 5364–5370.

Li, J.Y., Dunn, M.L., 1998a. Anisotropic coupled-field inclusion and inhomogeneity problems. Philos. Mag. A 77, 1341–1350.

Li, J.Y., Dunn, M.L., 1998b. Micromechanics of magnetoelectroelastic composite materials: Average fields and effective properties. J. Intel. Mater. Syst. Struct. 9, 404–416.

Li, J.Y., 2000. Magnetoelectroelastic multi-inclusion and inhomogeneity problems and their applications in composite materials. Int. J. Eng. Sci. 38, 1993–2011.

Shabana, Y.M., 2003. Incremental constitutive equation for discontinuously reinforced composites considering reinforcement damage and thermoelasto plasticity. Comput. Mater. Sci. 28, 31–40.

Sosa, H., 1992. On the fracture mechanics of piezoelectric solids. Int. J. Solids Struct. 29, 2613–2622.

Tang, T., Yu, W., 2009. Micromechanical modeling of the multiphysical behavior of smart materials using the variational asymptotic method. Smart Mater. Struct. 18, 1–14.

Tohgo, K., Chou, T.W., 1996. Incremental theory of particulate-reinforced composites including debonding damage. JSME Int. J. Ser. A 39, 389–397.

Wu, T.L., Huang, J.H., 2000. Closed-form solutions for the magnetoelectric coupling coefficients in fibrous composites with piezoelectric and piezomagnetic phases. Int. J. Solids Struct. 37, 2981–3009.

Zhong, Z., Meguid, S.A., 1997. Interfacial debonding of a circular inhomogeneity in piezoelectric materials. Int. J. Solids Struct. 34, 1965–1984.